Experimental Setup and Learning-Based AI Model for Developing Accurate PV Inverter Models

Preprint

Salma Bennai,[1] Kumaraguru Prabakar,[1] Yaswanth Nag Velaga,[1] Subhankar Ganguly,[1] Deepthi Vaidhynathan,[1] Matthew Reynolds,[1] Jonathan Frantz,[1] and Karthikeyan Balasubramaniam[2]

1 National Renewable Energy Laboratory
2 Argonne National Laboratory

Presented at the 2024 IEEE Kansas Power & Energy Conference
Manhattan, Kansas
April 25–26, 2024

NREL is a national laboratory of the U.S. Department of Energy
Office of Energy Efficiency & Renewable Energy
Operated by the Alliance for Sustainable Energy, LLC

This report is available at no cost from the National Renewable Energy Laboratory (NREL) at www.nrel.gov/publications.

Contract No. DE-AC36-08GO28308

Conference Paper
NREL/CP-5D00-89562
September 2024

Experimental Setup and Learning-Based AI Model for Developing Accurate PV Inverter Models

Preprint

Salma Bennai,[1] Kumaraguru Prabakar,[1] Yaswanth Nag Velaga,[1] Subhankar Ganguly,[1] Deepthi Vaidhynathan,[1] Matthew Reynolds,[1] Jonathan Frantz,[1] and Karthikeyan Balasubramaniam[2]

1 National Renewable Energy Laboratory
2 Argonne National Laboratory

Suggested Citation
Bennai, Salma, Kumaraguru Prabakar, Yaswanth Nag Velaga, Subhankar Ganguly, Deepthi Vaidhynathan, Matthew Reynolds, Jonathan Frantz, and Karthikeyan Balasubramaniam. 2024. *Experimental Setup and Learning-Based AI Model for Developing Accurate PV Inverter Models: Preprint*. Golden, CO: National Renewable Energy Laboratory. NREL/CP-5D00-89562. https://www.nrel.gov/docs/fy24osti/89562.pdf.

NREL is a national laboratory of the U.S. Department of Energy
Office of Energy Efficiency & Renewable Energy
Operated by the Alliance for Sustainable Energy, LLC

This report is available at no cost from the National Renewable Energy Laboratory (NREL) at www.nrel.gov/publications.

Contract No. DE-AC36-08GO28308

Conference Paper
NREL/CP-5D00-89562
September 2024

National Renewable Energy Laboratory
15013 Denver West Parkway
Golden, CO 80401
303-275-3000 • www.nrel.gov

NOTICE

This work was authored in part by the National Renewable Energy Laboratory, operated by Alliance for Sustainable Energy, LLC, for the U.S. Department of Energy (DOE) under Contract No. DE-AC36-08GO28308. This material is based upon work supported by the U.S. Department of Energy's Office of Energy Efficiency and Renewable Energy (EERE) under Solar Energy Technologies Office (SETO) Agreement Number 38455. A portion of the research was performed using computational resources sponsored by the U.S. Department of Energy's Office of Energy Efficiency and Renewable Energy and located at the National Renewable Energy Laboratory. The views expressed herein do not necessarily represent the views of the DOE or the U.S. Government.

Cover Photos by Dennis Schroeder: (clockwise, left to right) NREL 51934, NREL 45897, NREL 42160, NREL 45891, NREL 48097, NREL 46526.

Experimental Setup and Learning-Based AI Model for Developing Accurate PV Inverter Models

Salma Bennai, Kumaraguru Prabakar, Yaswanth Nag Velaga, Subhankar Ganguly, Deepthi Vaidhynathan, Matthew Reynolds, Jonathan Frantz, National Renewable Energy Laboratory, Golden, CO, USA
kumaraguru.prabakar@nrel.gov

Karthikeyan Balasubramaniam, Argonne National Laboratory, Argonne, IL, USA

***Abstract*— The integration of power electronics-based interfaces presents challenges due to the absence of detailed models and the high computational complexity. Generic models used in system studies lack accuracy in capturing converter dynamics. This paper proposes a data-driven approach developed from experimental setup data. This approach enhances accuracy in photovoltaic inverter modeling. We used two types of PV inverters in the experiment. The recorded experimental data undergo processing through a machine learning model. Results from the model trained through machine learning is also presented.**

Keywords—Inverters, inverter under test, inverter black box model, machine learning, artificial intelligence, experimental setup.

I. Introduction

The increase of power electronics-based generation requires accurate converter modeling as solar photovoltaic (PV) inverters are becoming a key distributed energy resource. Yet, widely used generic inverter models in grid studies are oversimplified, lack accuracy, and fail to represent real converters with multiple dynamic subsystems, hierarchical control, and communication systems [1], [2].

One of the approaches to the problem is developing a black box model that can be fully parameterized by experimentally evaluating the converter response. Previous works have proposed the use of artificial neural Network-based IBR modeling. Authors in [3], [4], [5] used ANN to train and model commercial photovoltaic microinverters by converting time domain data from power Hardware-in-the-Loop (PHIL) into the frequency domain. Others in [6], [7] use ANN to build impedance models and proposed the techniques to solve operating point-dependent challenges

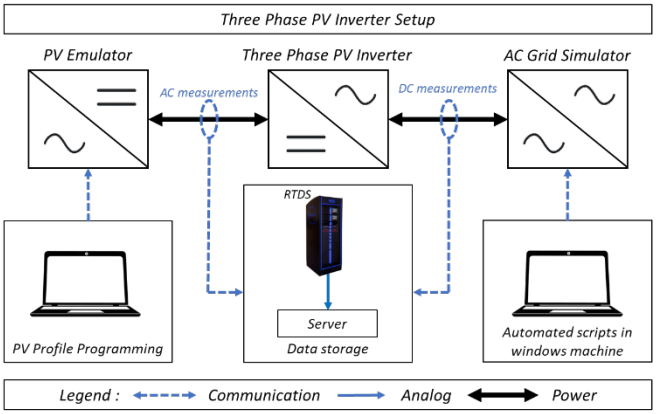

Fig. 1. Inverter under test experimental setup.

This paper presents a data-driven approach to identify an accurate inverter model using an experimental setup with two off-the-shelf commercial inverters. A learning-based approach is used to accurately represent the inverter under test (IUT) behavior using recorded experimental data [3]. The experimental setup is detailed and serves as a template for testing utility-scale converters. The generated data are publicly available, enabling researchers to develop accurate converter models [8], [9], [10].

This paper details our contribution to generating datasets, formulating model architecture, and training models using high-performance computing. Emphasis is on our data collection through power hardware-in-the-loop experiments that have enabled us to use empirical datasets in contrast to simulated data used to train converter data-driven models.

II. Experimental Setup to Collect Data

This paper uses both a three-phase PV inverter and a split-phase PV IUT for the experiments, as shown in Fig. 1. Both setups consist of a grid simulator, AC measurement box, IUT, DC measurement box, and DC power supply (PV emulator). Real-Time Digital Simulator (RTDS) and analog input cards facilitate the data collection. The first setup features a three-phase PV inverter with a 600-V/25-A input curve, and the second setup employs a split-phase PV inverter with a 600-V/15-A input curve. The PV emulator adjusts the irradiance levels from 100% to 75%, 50%, and 25%, while the grid simulator maintains constant voltage and frequency. A Python script automates the grid simulator control, synchronizing the irradiance changes with grid voltage and frequency adjustments. The flowchart of the experiment is shown in Fig. 2.

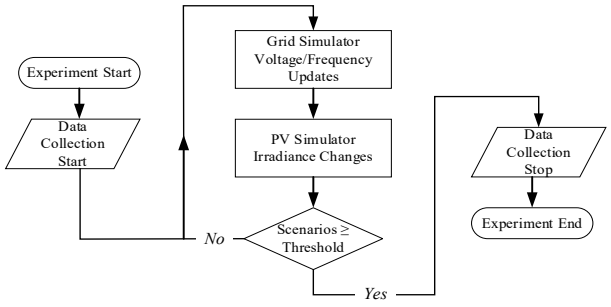

Fig. 2. Experiment flowchart.

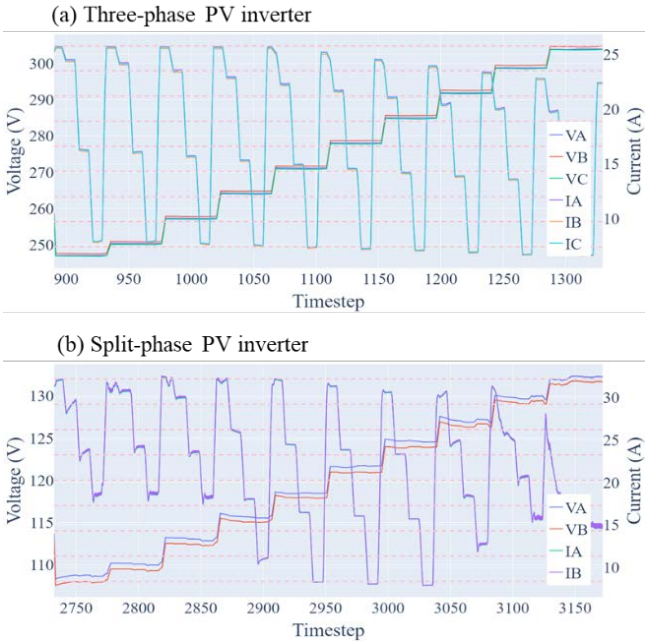

Fig. 3. AC voltage and current RMS over time (s)—(a) y-axis (left): voltage A, B, C (V), current A, B, C (A); (b) y-axis (left): voltage A, B (V), current A, B (A)

A. *Voltage Run*

The voltage ranges from 0.9 to 1.1 p.u. in 0.025-p.u. increments, maintaining a constant 60-Hz frequency. Data for the three-phase PV inverter were sampled every 1 ms for 442.241 s and for the split-phase PV inverter every 1 ms for 442.1885 s. Fig. 3 illustrates the AC voltage and current.

In both setups, the voltage and current samples were squared, subjected to a rolling average, and the square root was taken for each, with one sample chosen from every 100 samples. In the three-phase setup, the reference voltages ranged from 0.9 to 1.1 p.u. In the split-phase setup, the reference voltages varied from 0.9 to 1.1 times 120 V with 3-V steps.

The three-phase PV inverter root-mean-square (RMS) voltage amplitudes range from 247 V to 304 V between reference voltages (see Table I), with Voltage B exceeding Voltage A by 0.5 V and Voltage C by 0.8 V. The current RMS amplitudes range from 6.7 A to 25.7 A, with Current A exceeding Current C by 0.1 A and Current B by 0.2 A. In the split-phase setup, the RMS voltage amplitudes vary from 108 V to 132 V between the reference voltages, with Voltage A surpassing Voltage B by 0.7 V. The RMS current ranges from 7.9 A to 32.5 A (see Table II).

Fig. 4 illustrates the DC voltage and current for both the three-phase and split-phase PV inverters with the data sampled at intervals of 1 in every 100 samples.

In the three-phase system, the DC voltage and current has a repeating pattern every 43 s, with the voltage ranging from 843 V to 956 V and the current from 7.3 A to 28.2 A (see tables III and IV). In the split-phase system, a loosely repeating pattern occurs every 44 s, with the DC voltage varying from 338 V to 418 V and the DC current fluctuating between 1.6 A and 23.4 A (see tables III and IV). Fig. 5 shows the AC voltage, with the data truncated to show only the first 1/60 samples.

TABLE I AC RMS VOLTAGE

Three-phase PV inverter										
$t(s)$	891	934	978	1022	1066	1110	1154	1198	1242	1286
V_{Before} (V)	–	247	250	257	264	271	278	285	292	299
V_{After} (V)	247	250	257	264	271	278	285	292	299	304
Split-phase PV inverter										
$t(s)$	2733	2776	2820	2864	2908	2952	2996	3040	3084	3128
V_{Before} (V)	–	247	250	257	264	271	278	285	292	299
V_{After} (V)	247	250	257	264	271	278	285	292	299	304

TABLE II AC RMS CURRENT

Three-phase PV inverter										
$t(s)$	891	930	973	1016	1059	1102	1145	1188	1231	1247
I_{Before} (V)	–	8.0	8.0	7.7	7.5	7.4	7.2	7.1	6.9	6.7
I_{After} (V)	25.7	25.7	25.7	25.6	25.6	25.1	24.5	23.9	23.3	22.8
Split-phase PV inverter										
$t(s)$	2733	2773	2817	2861	2905	2949	2993	3037	3081	3125
I_{Before} (V)	–	19.7	18.8	18.2	11.1	8.3	8.1	7.9	12.9	15.6
I_{After} (V)	32.0	31.9	32.5	32.2	31.6	31.7	30.9	30.3	31.4	28.1

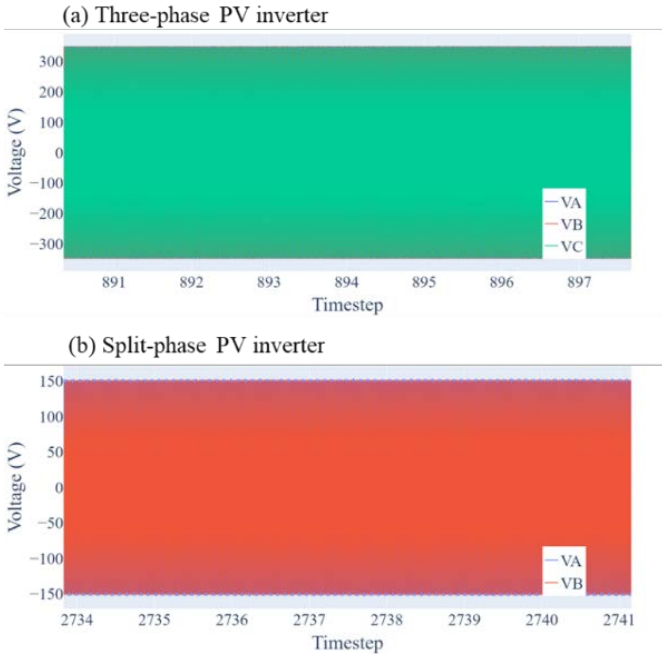

Fig. 4. AC voltage truncated over time (s)—(a) y-axis: voltages A, B, and C (V), (b) y-axis: voltages A and B (V)

In the three-phase PV inverter setup, the AC voltages are three phase waveform each at approximately 60 Hz and phase-shifted by 120° from one another. The amplitudes of these waves remain constant within a selected portion. Similarly, in the split-phase PV inverter setup, the observed voltages are bi-phase waveforms, each at approximately 60 Hz and phase-shifted by 180° from one another. The amplitudes of these waves also remain constant within the selected portion.

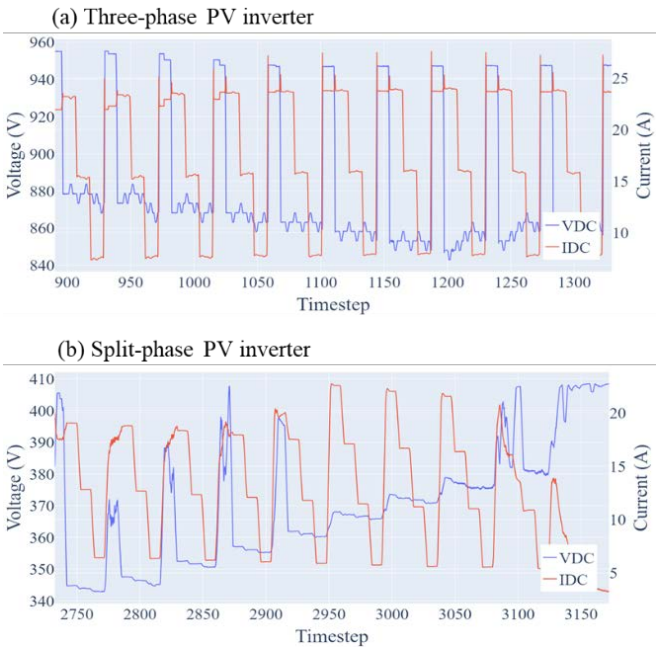

Fig. 5. DC voltage and current over time (s)—y-axis (left): voltages (V), y-axis (right): currents (A)

TABLE III DC VOLTAGE

Three-phase PV inverter										
$t(s)$	929	972	1015	1058	1101	1144	1187	1230	1273	1322
$V_{Before}\ (V)$	874	869	869	863	859	853	848	853	859	856
$V_{After}\ (V)$	955	954	951	948	947	947	947	947	947	947
Split-phase PV inverter										
$t(s)$	2733	2773	2818	2862	2906	2950	2994	3038	3082	3126
$V_{Before}\ (V)$	–	343	345	351	355	360	366	371	376	380
$V_{After}\ (V)$	405	367	388	398	398	368	374	379	392	390

TABLE IV DC CURRENT

Three-phase PV inverter										
$t(s)$	929	972	1015	1058	1101	1144	1187	1230	1273	1322
$V_{Before}\ (V)$	7.6	7.7	7.6	7.8	7.8	7.9	8.0	8.0	7.9	7.9
$V_{After}\ (V)$	25.0	25.1	25.9	27.2	27.5	27.5	27.6	27.5	27.2	27.3
Split-phase PV inverter										
$t(s)$	2733	2773	2818	2862	2906	2950	2994	3038	3082	3126
$V_{Before}\ (V)$	–	6.5	6.4	6.2	6.1	5.9	5.8	5.6	5.6	5.4
$V_{After}\ (V)$	17.9	16.1	17.0	15.7	20.4	22.7	22.3	21.8	20.7	13.6

B. *Frequency Run*

In the frequency run experiments, the frequency is varied in steps at 59.4 Hz, 59.6 Hz, 59.8 Hz, 60.2 Hz, 60.4 Hz, and 60.45 Hz while maintaining a constant voltage amplitude of 1 p.u. In the three-phase PV inverter setup, data were recorded at 1-ms intervals over 247.653 s. In the split-phase PV inverter setup, data were recorded at 1 ms intervals for 247.968 s. Figs. 6 and 7 depict the Phase A voltage and current using a computed short-time Fourier transform (STFT) for the frequency domain analysis at various intervals. The color in the figures represents the signal's amplitude within the frequency bucket over time.

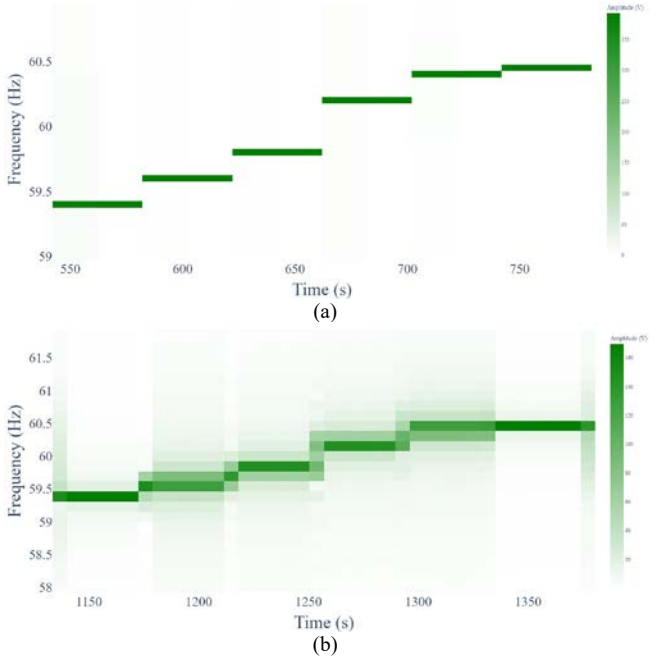

Fig. 6. Frequency of Phase A voltage

The STFT involves applying a window input function, performing the Fourier transform, and repeating the process with window shifts. For Figs. 6 and 7 (a) with amplitude prioritized, a 20,000-point discrete Fourier transform (DFT) with a rectangular window is computed every 20,000 samples.

In Figs. 6 and 7 (b) prioritizing amplitude, a 5,000-point DFT with a rectangular window is computed every 5,000 samples. For Fig. 6 (a) with time prioritized, a 20,000-point DFT with a Gaussian window is computed every 500 samples. In Fig. 7 (a) prioritizing time, a 40,000-point DFT with a Gaussian window is computed every 500 samples. For Figs. 6 and 7 (b) prioritizing time, a 25,000-point DFT with a Gaussian window is computed every 1,250 samples.

In the three-phase PV inverter setup, the signal shows discrete frequency jumps between 59.4 Hz, 59.6 Hz, 59.8 Hz, 60.2 Hz, 60.4 Hz, and 60.45 Hz at specific times (see Table V) as programmed in the controllable supply. Similarly, in the split-phase PV inverter setup, the signal undergoes discrete frequency transitions, briefly reaching 60 Hz and then switching between 59.4 Hz, 59.6 Hz, 59.8 Hz, 60.2 Hz, 60.4 Hz, and 60.45 Hz, as shown in Table V.

In this paper, we used the three phase PV inverter data set to train a model. Split phase inverter data was not used for the training. Trained split phase inverter model will be presented in a different report.

TABLE V VOLTAGE AND CURRENT FREQUENCY

Three-phase PV inverter					
$t(s)$	580	622	663	704	743
$f_{Before}\ (Hz)$	59.4	59.6	59.8	60.2	60.4
$f_{After}\ (Hz)$	59.6	59.8	60.2	60.4	60.45
Split-phase PV inverter					
$t(s)$	1170	1212	1255	1297	1338
$f_{Before}\ (Hz)$	59.4	59.6	59.8	60.2	60.4
$f_{After}\ (Hz)$	59.6	59.8	60.2	60.4	60.45

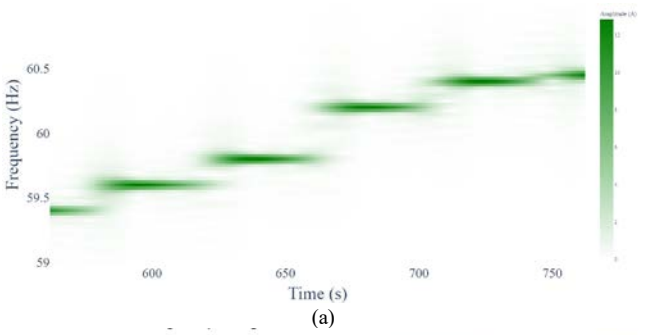

(a)

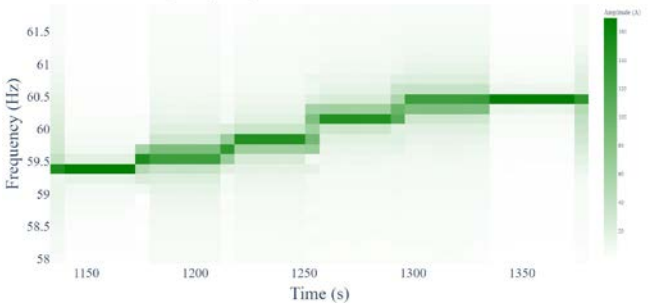

(b)

Fig. 7. Frequency of Phase A current

III. Machine Learning Setup

Central to developing accurate PV inverter models is building a mapping from input to output variables. Specifically for this paper, a mapping from the three-phase voltage, DC current, and DC voltage to the three-phase current was built using a simple feed-forward neural network with two hidden layers. The reason for choosing this model was to demonstrate that accurate inverter models can be built even with simple models such as standard feed-forward neural networks. Setting up and training such a model is fast and straightforward using libraries such as TensorFlow using the Keras interface, which was used in this paper. The rest of this section briefly describes the architecture and training of the neural network PV inverter model.

The workflow for training the machine learning model is illustrated in Fig. 8. Each step in Fig. 8 is described in detail in the following discussion. First, data collected from the inverters were first preprocessed, i.e., first split into training and testing data, and the training data were subsequently normalized. Once the data preprocessing step was completed, the neural network architecture was chosen. The neural network PV inverter model architecture consists of an input layer with five inputs: three-phase voltage (a, b, c), DC current, and DC voltage. and the resulting input layer was connected to two layers (fully connected) consisting of 100 nodes each.

Rectified linear activation functions were used (see, e.g., [11]) for the hidden layers, and, finally, the last hidden layer was connected to an output layer consisting of three nodes, one for each phase of the three-phase output current.

For training the neural network, mean-squared error was selected for the loss function, and an Adam optimizer was employed [11] to fit the data using 100 epochs as a termination condition. After the 100 epochs of training completed, the authors determined that no further training or updates to the neural network architecture were required, and the model was evaluated against the test data set. The results of the training, including the mean-squared error loss values for the training and test data, are shared in the next section.

The data set for the voltage step change experiments were split into a training data set consisting of two-thirds of the data and the testing data set consisting of one-third of the data. Because the data consist of time-series output, the test-train split was performed by taking the first two-thirds of the data for training and the last one-third for testing instead of a randomized split across the extent of the data.

We emphasize the utility of a simple machine learning-based PV inverter model: The goal was to demonstrate that useful results can be obtained even using basic (and not finely tuned) machine learning models that are easily trained. Indeed, this model should be improved upon in practice, and the authors encourage interested readers to experiment with more advanced neural network topologies and machine learning methodologies, and to finely tune their models, with the goal of improving upon the results demonstrated in this paper.

IV. Machine Learning Results

For the voltage step example, training the neural networks for 100 epochs resulted in an average mean-squared error (averaged over the three phases) loss of 0.0104 for the training data and 0.0838 for the test data. For the frequency step example, training the neural networks for 100 epochs resulted in an average mean-squared error loss of 0.0762 for the training data and 0.0655 for the test data. Outputs from the machine learning models trained using the voltage step and frequency step data sets are shown in Figs. 9 to 12, respectively.

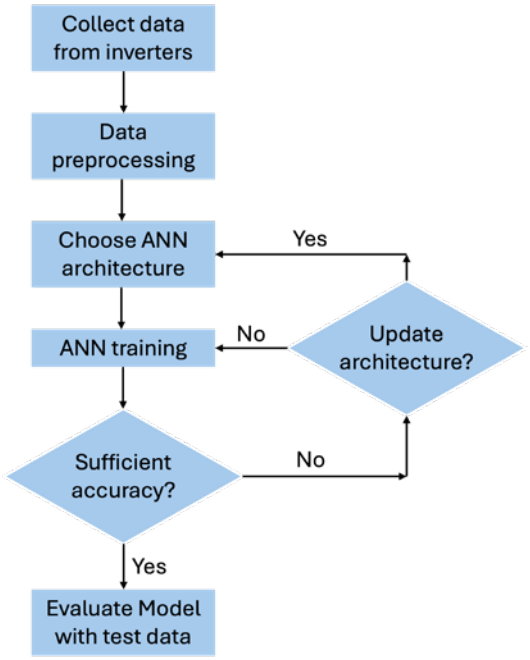

Fig. 8. Machine learning workflow for training artificial neural networks (ANNs).

After 100 epochs of training, the models built using the voltage step and frequency step data capture the major features contained within the output current data sets; however, there is still room for improvement. In both models, near the tops of the oscillations (see Figs. 9 and 11), there are visible over- and undershoots. Further, it is evident from the zoom-in on the Phase C data from Fig. 10 that the model trained using the frequency step data could potentially benefit from further training. Visible in Fig. 9, the model also misses some events in the final third of the time-series data. Recalling that the final third of the time-series data were kept out of the model training, the plots in Fig. 9 suggest that the training data might not have provided sufficient information for the model to capture such events. At this time, more investigation is required to understand whether a lack of sufficient training data, an insufficient model architecture, or an insufficiently trained model are responsible for the model missing the events in the final third of the time steps in Fig. 9.

V. Conclusion

This paper presented a novel method for accurately modeling PV inverters using experimental data processed through a machine learning-based model. The model employs measured voltages, and currents as input data to predict the

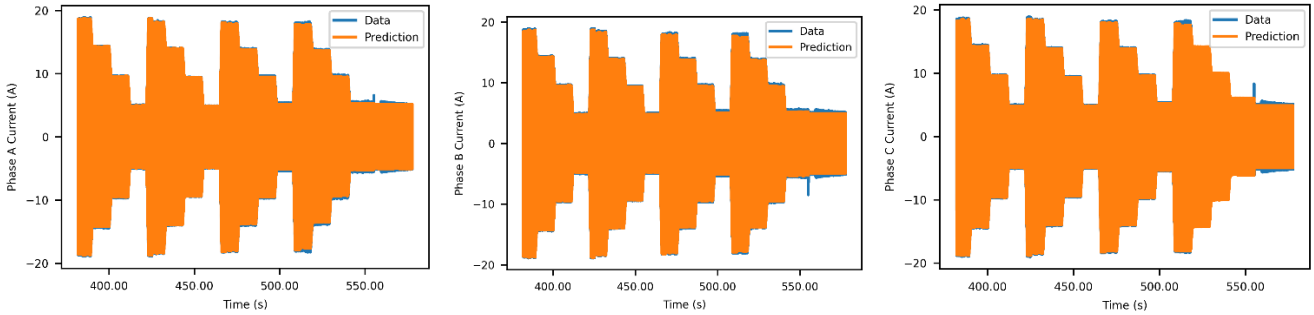

Fig. 9. Three-phase (a, b, c) current from voltage step experiments overlaid with AI-based PV inverter model output.

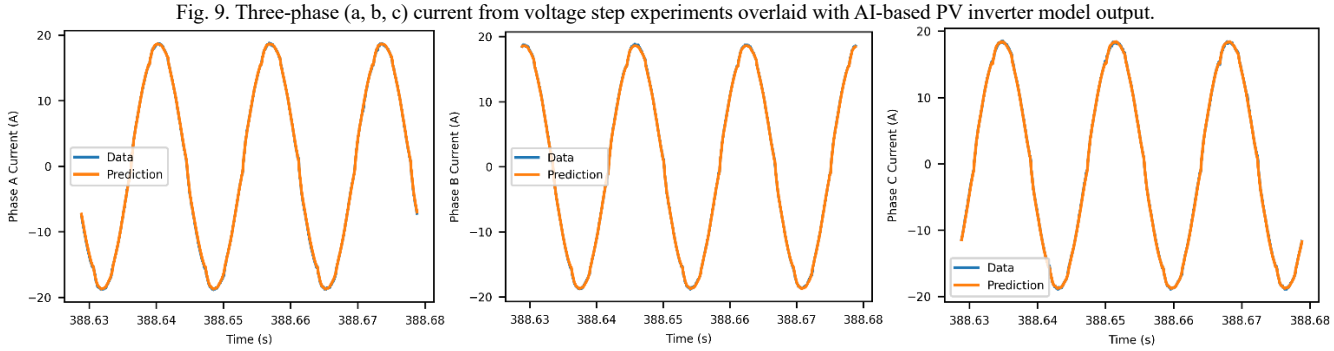

Fig. 10. Three-phase (a, b, c) current zoomed in from voltage step experiments overlaid with AI-based PV inverter model output.

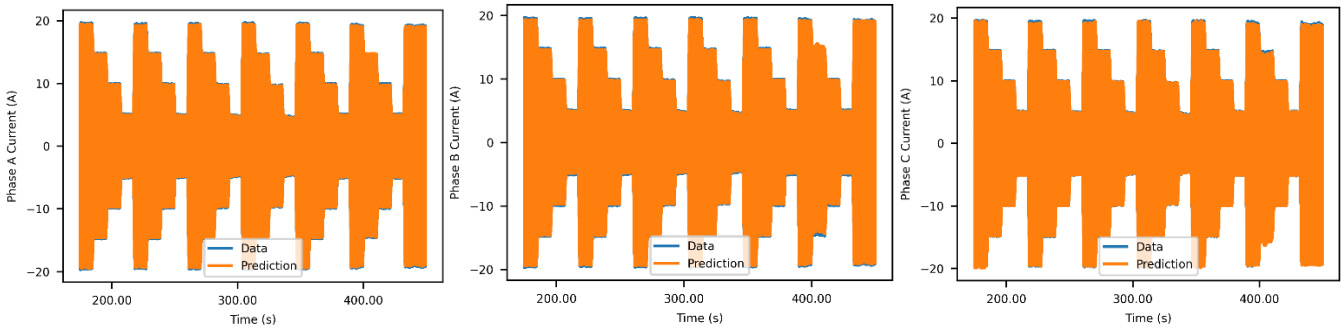

Fig. 11. Three-phase (a, b, c) current from frequency step experiments overlaid with AI-based PV inverter model output.

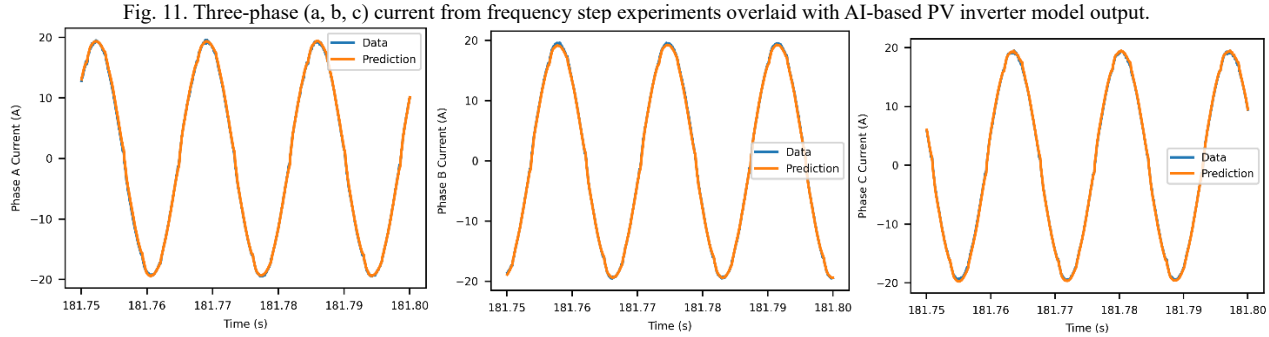

Fig. 12 Three-phase (a, b, c) current zoomed in from frequency step experiments overlaid with PV inverter model output.

optimal current representing the IUT's behavior. The inverter model is developed using TensorFlow via the Keras interface. The currents are generated through a neural network application programming interface. Using a simple feed-forward architecture with two fully connected hidden layers, the model accurately reproduces most of the events contained in the output current; however, some events in the test data were missed, and more work is required to understand how to update the model to capture such events while avoiding overfitting.

Future work on this topic will include experimenting with more advanced neural network architectures and more carefully tuning the machine learning model. Convolutional neural networks and long short-term memory-based networks both present interesting paths forward in terms of new models to use with these data sets [11].

VI. Acknowledgments

This work was authored in part by the National Renewable Energy Laboratory, operated by Alliance for Sustainable Energy, LLC, for the U.S. Department of Energy (DOE) under Contract No. DE-AC36-08GO28308. This material is based upon work supported by the U.S. Department of Energy's Office of Energy Efficiency and Renewable Energy (EERE) under Solar Energy Technologies Office (SETO) Agreement Number 38455. The views expressed in the article do not necessarily represent the views of the DOE or the U.S. Government. The U.S. Government retains and the publisher, by accepting the article for publication, acknowledges that the U.S. Government retains a nonexclusive, paid-up, irrevocable, worldwide license to publish or reproduce the published form of this work, or allow others to do so, for U.S. Government purposes. A portion of the research was performed using computational resources sponsored by the U.S. Department of Energy's Office of Energy Efficiency and Renewable Energy and located at the National Renewable Energy Laboratory..

VII. References

[1] "WECC Base Case Review: Inverter-Based Resources," NERC-WECC Joint Report, Atlanta, GA, USA, Aug. 2020.

[2] J. Xie and T. McDermott, "Generic EMT Modeling for IBR," PNNL--35064, 2007764, Jan. 2023. doi: 10.2172/2007764.

[3] L. Fan, Z. Miao, S. Shah, P. Koralewicz, V. Gevorgian, and J. Fu, "Data-Driven Dynamic Modeling in Power Systems: A Fresh Look on Inverter-Based Resource Modeling," *IEEE Power and Energy Mag.*, vol. 20, no. 3, pp. 64–76, May 2022, doi: 10.1109/MPE.2022.3150827.

[4] E. Kaufhold, S. Grandl, J. Meyer, and P. Schegner, "Feasibility of Black-Box Time Domain Modeling of Single-Phase Photovoltaic Inverters Using Artificial Neural Networks," *Energies*, vol. 14, no. 8, p. 2118, Apr. 2021, doi: 10.3390/en14082118.

[5] N. Guruwacharya *et al.*, "Data-driven Modeling of Commercial Photovoltaic Inverter Dynamics Using Power Hardware-in-the-Loop," in *2022 International Symposium on Power Electronics, Electrical Drives, Automation and Motion (SPEEDAM)*, Sorrento, Italy: IEEE, Jun. 2022, pp. 924–929. doi: 10.1109/SPEEDAM53979.2022.9842001.

[6] M. Zhang, X. Wang, and Q. Xu, "Data-Driven Modeling of Power-Electronics-Based Power System Considering the Operating Point Variation," in *2021 IEEE Energy Conversion Congress and Exposition (ECCE)*, Vancouver, BC, Canada: IEEE, Oct. 2021, pp. 3513–3517. doi: 10.1109/ECCE47101.2021.9595218.

[7] M. Zhang, X. Wang, D. Yang, and M. G. Christensen, "Artificial Neural Network Based Identification of Multi-Operating-Point Impedance Model," *IEEE Trans. Power Electron.*, vol. 36, no. 2, pp. 1231–1235, Feb. 2021, doi: 10.1109/TPEL.2020.3012136.

[8] Kumaraguru Prabakar, Subhankar Ganguly, Yaswanth Nag Velaga, and Deepthi Vaidhynathan, "PV inverter experimental data," Golden, CO: National Renewable Energy Laboratory, Dec. 2023. doi: 10.7799/1914317.

[9] Kumaraguru Prabakar, Subhankar Ganguly, Yaswanth Nag Velaga, and Deepthi Vaidhynathan, "Split phase inverter data," Golden, CO: National Renewable Energy Laboratory, Dec. 2023. doi: 10.7799/1962803.

[10] Kumaraguru Prabakar, Subhankar Ganguly, Yaswanth Nag Velaga, and Deepthi Vaidhynathan, "Battery inverter experimental data," Golden, CO: National Renewable Energy Laboratory, Dec. 2023. doi: 10.7799/1908195.

[11] Ian Goodfellow, Yoshua Bengio, and Aaron Courville, *Deep Learning*. MIT Press, 2016. [Online]. Available: https://www.deeplearningbook.org/